Dynamic outgassing of deuterium, helium and nitrogen from plasma-facing materials under DEMO relevant conditions

2017 Nucl. Fusion 57 016020

(http://iopscience.iop.org/0029-5515/57/1/016020)

OPEN ACCESS
IOP Publishing | International Atomic Energy Agency
Nuclear Fusion
Nucl. Fusion **57** (2017) 016020 (10pp)
doi:10.1088/0029-5515/57/1/016020

Dynamic outgassing of deuterium, helium and nitrogen from plasma-facing materials under DEMO relevant conditions

S. Möller[a], D. Matveev, Y. Martynova, B. Unterberg, M. Rasinski, T. Wegener, A. Kreter and Ch. Linsmeier

Forschungszentrum Jülich GmbH, Institut für Energie- und Klimaforschung—Plasmaphysik, Partner of the Trilateral Euregio Cluster (TEC), 52425 Jülich, Germany

E-mail: s.moeller@fz-juelich.de

Received 19 August 2016, revised 27 September 2016
Accepted for publication 5 October 2016
Published 1 November 2016

Abstract

In confined plasma magnetic fusion devices significant amounts of the hydrogen isotopes used for the fusion reaction can be stored in the plasma-facing materials by implantation. The desorption of this retained hydrogen was seen to follow a t^{α} law with $\alpha \approx -0.7$ in tokamaks. For a pulsed fusion reactor this outgassing can define the inter-pulse waiting time. This work presents new experimental data on the dynamic outgassing in ITER grade tungsten exposed under the well-defined conditions of PSI-2 to pure and mixed D_2 plasmas.

A peak ion flux of 10^{22} D^+ m^{-2} s is applied for up to 6 h at sample temperatures of up to 900 K. Pure D_2 and mixed $D_2 + He$, $D_2 + N_2$ and $D_2 + He + N_2$ plasmas are applied to the sample at 68 V bias. The D_2, He, N outgassing at 293 K and 580 k are observed via in-vacuo quadrupole mass spectrometry covering the range of 40 s–200 000 s after exposure.

The outgassing decay follows a single power law with exponents $\alpha = -0.7$ to -1.1 at 293 K, but at 580 K a drop from $\alpha = -0.25$ to -2.35 is found. For DEMO a pump-down time to 0.5 mPa in the order of 1–5 h can be expected. The outgassing is in all cases dominated by D_2.

Keywords: hydrogen retention, tungsten, plasma-surface-interaction, dynamic inventory, outgassing, PSI-2, DEMO

(Some figures may appear in colour only in the online journal)

1. Introduction

The implantation and subsequent retention and outgassing of hydrogen in metals, especially tungsten (W), is relevant for the development of nuclear fusion as a power source. Several effects as material embrittlement, fuel recycling and tritium self-sufficiency are influenced by the retention and loading of in-vessel materials with hydrogen. The hydrogen loading density and thus the relevance of these effects can strongly depend on the material, temperature, radiation damage and plasma parameters. Besides these material related issues a commercial tokamak reactor can be limited in its duty cycle if the pump-down of the vacuum vessel to the start-up base pressure takes a significant amount of time.

Several aspects of the long-term retention mechanisms have been understood via experimental verification of codes as TMAP, see e.g. [1]. The density of retained deuterium was quantified in several conditions. Depth profiles of the long-term D retention in W were obtained. A coupling between apparent diffusion coefficient and hydrogen loading, induced by trapping at crystal defects, was discovered [2]. This effect is sometimes also called anomalous diffusion and is induced by the barrier effect of trapping sites. Discrepancies between TMAP predictions of the outgassing and the observations were observed [2].

[a] Author to whom all correspondence should be addressed.

The hydrogen in the material can occupy two different types of sites at a given temperature. On the one hand hydrogen bound to sites with binding energies below the available thermal energy is called dynamic retained. In tungsten at room temperature these are probably interstitial sites with about 0.2–0.4 eV [3] and a naturally high volume density. On the other hand higher binding energy states can exist which are stable at the given temperature, which is then called long-term retention or just retention. In tungsten energies of 1 to 2 eV are associated with this [4]. On short timescales (up to several hours) after plasma exposure, when the hydrogen content is not in equilibrium and thus the dynamic inventory is at least partially filled open questions remain. The depth distribution and density of retained D can depend on the balance between influx of D from the plasma and outflux by diffusion and surface recombination (desorption).

Studies indicated a diffusion limited regime is present in the case of D in W [5]. The outgassing in the JET tokamak was seen to follow a power law with time ($t^{-0.7}$) with carbon and metal walls alike [6, 7]. Two approaches for theoretical understanding are present. The model presented in [6] assumes that the power law is an effective relation, arising from the mixture of several local exponential functions in large devices. On the other hand the model presented in [8] relates the behaviour to fundamental aspects of outgassing related to hydrogen binding states. The combination of reaction-diffusion equations provides a physically solid basis [9]. From detailed code based analysis it is claimed that the power law is only on short scales a valid description, arising from smearing due to experimental uncertainties, the development of depth profiles and certain ratios between diffusion and recombination [10]. More complex situations where helium is present in the plasma and seeding gases are injected to cool the plasma boundary are even less understood. Helium is reducing the long-term retention of hydrogen [11], but the outgassing of the helium itself contributes also to the total pressure in the vessel. Nitrogen as a candidate seeding gas for plasma-edge cooling produces nitrides with tungsten which may have totally different rates of hydrogen diffusion and surface recombination.

In this work the outgassing after exposure to pure and mixed D_2 plasmas under conditions relevant for a DEMO reactor is addressed. Extrapolations are applied to use the experimental results for the calculation of the pressure and pump-down in the phase between to plasma discharges. The applicability of existing modelling for pure D_2 exposures to the new situations is discussed.

2. Experimental

For the presented experiments the hot-cathode linear arc-plasma device PSI-2 is used to ensure a minimum complexity of the experimental setup. The details of the device were described e.g. in [12]. High purity D_2 and mixed plasmas are employed by introducing D_2 gas with 99.8% (99.9999% D + H), He 99.9995% and nitrogen with 99.8% purity. The PSI-2 base pressure is $8 \pm 3 * 10^{-8}$ mbar (dominated by H_2O) in all experiments, so a small impurity content is present. From working gas influx considerations the impurity ratio can be estimated to be in the order of 10^{-5}. The samples are exposed on the axial manipulator. Rough $100 \times 80\,\mathrm{mm}^2$ W plates (99.96% purity) are used in the experiments (see figure 1).

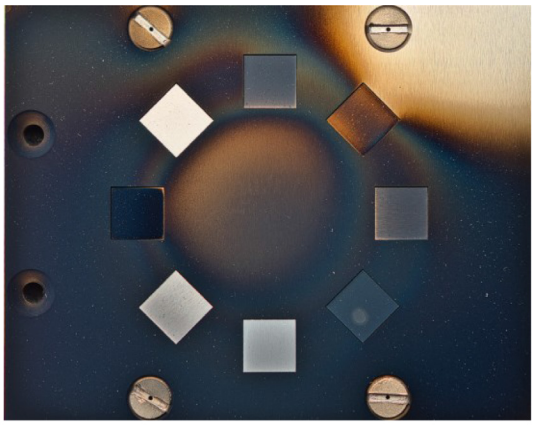

Figure 1. Sample holder after the D_2 + He irradiation. Blackening by fuzz is visible, but some samples are up to 300 K hotter during exposure, as indicated by the IR camera, leading to destruction of the fuzz. The colored ring around the centre marks the position of the peak plasma flux. The polished sample on the left is post-analysed.

The outgassing analysis is done in-vacuo in the target exchange and analysis chamber (TEAC), see figure 2. The samples are transferred via a manipulator from the exposure position to TEAC within 50 s in the first and 30 s in the last experimental set. The gas transfer between plasma chamber and TEAC is limited, ensuring that the pressure in TEAC is always $\leqslant 1 \pm 0.3\ ^{*}\ 10^{-6}$ mbar. TEAC is equipped with a 1300 l s^{-1} (for Helium/D_2) Pfeiffer HiPace 1200 turbo-molecular pump. For $m/z = 4$ an e-folding pump-down time of 58 ± 2 ms is measured at 630 Hz pump rotation speed. The pump-down to the D_2 background order takes about 10 s, see figure 4, so the first relevant data-point is collected 40 s/60 s after the plasma exposure. Spikes in the outgassing data, especially visible for gases present in air, are due to a known deficit in current rotary vane pump technology. As the spikes are as short as the pumping time and have a frequency of about one per 30 min, their influence is neglected.

In the case of active pumping during outgassing the quasi-static partial pressure is governed by

$$F = \frac{\mathrm{d}P}{\mathrm{d}t} * \frac{V}{k_\mathrm{B}T} + \frac{S * P}{k_\mathrm{B}T} \tag{1}$$

$$\Rightarrow F \approx \frac{S * P}{k_\mathrm{B}T} \tag{2}$$

where V is the vacuum vessel volume, S the pumping speed in volume per second, P the partial pressure of the considered gas species and F the outgassing flux of that species. With the small volume of TEAC of about 0.08 m^3 and the comparably high pumping speed, the volume times pressure drop rate term of equation (1) becomes small (~10^{-3}–10^{-5}) compared to the second term. For this reason a direct interpretation of measured partial pressure signals as outgassing flux becomes possible (equation (2)), in contrast to the situation in Tokamaks where V/S can be 1000 times larger [6].

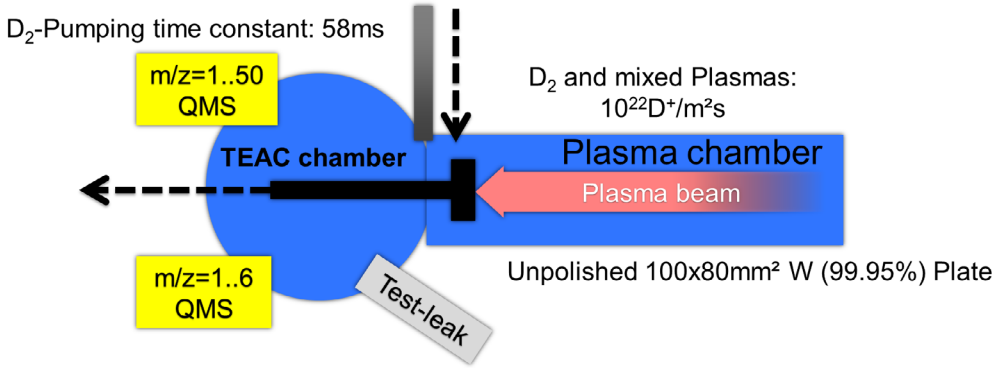

Figure 2. Experimental setup. After the plasma exposure the sample holder (black T) is retracted and the chamber is closed (grey bar) to obtain an environment free of chamber wall loading.

The partial pressures of volatile gases are analysed in a non-line-of-sight geometry using a Pfeiffer PrismaPlus QMG 220 M quadrupole mass spectrometer (QMS) and a MKS Microvision 2 triple filter for He/D_2 separation, both with Faraday and secondary electron multiplier (SEM) detectors. The mass over charge (m/z) values of 2, 3, 4, 18, 20, 28 (Prismaplus) and 4.0, 4.03 (Microvision) are analysed in each measurement. Fine tuning of the m/z values to the peak maxima is done prior to each measurement to compensate for device drifts. For each m/z peak an integration time of 500 ms, followed by a pause of 12 ms is used. For outgassing measurements the PSI-2 magnetic field is switched off, as it affects the QMS sensitivity. The outgassing flux is calibrated using a defined leak ($1 \pm 0.1 * 10^{-6}$ mbar $* 1\,s^{-1}$) with D_2, He and N_2 and assuming a linear connection between the QMS detector current and the partial pressure below a total pressure of 10^{-5} mbar, as linearity of the turbo-pump and QMS specifications suggest. The calibration leak signal of the Prismaplus ($4.3 \pm 0.2 * 10^{-11}$ A for D_2) varies only within 5% between the measurements, thus drifts during the measurements are assumed to be negligible for the Prismaplus. The Microvision shows relevant drifts in the data collection time thus it is only used for the short time where He outgassing is detected and D_2 outgassing is derived from the Prismaplus in all other cases.

The sample temperature is monitored using a type-K thermocouple attached to the sample back and an InSb-detector IR camera for relative information about the full surface. The sample is pre-heated to 600 K by a heater and further heated by the plasma exposure. According to finite element simulations the sample surface is about 10 K hotter during plasma exposure due to the frontal plasma heat load and the backside cooling contact. After plasma loading the sample is cooled down to a fixed temperature of 293 K/580 K. Heating and cooling have an exponential time constant of 110 ± 10 s. Pumping speeds and manipulator movement in PSI-2 do not allow monitoring the outgassing in the first 40 s after the exposure. As the usual power law fits to the outgassing yield an unphysical infinite outgassing rate for the moment directly after the exposure, this timeframe remains interesting, but so far inaccessible for the experiment.

Plasma currents and bias voltages with respect to the anode are measured at the sample manipulator to determine the integral ion flux density and ion impact energy. A reciprocating single tip Langmuir-probe is installed on top of the vessel in the centre of the plasma column 300 mm in front of the samples to measure spatially resolved radial profiles of flux density and electron temperature. The plasma is run with an input power of 14 kW (200 A arc current) and 100 sccm of D_2 + He gas injected into the source. If He is injected the inlet rate of 20 sccm leads to an ion fraction of 5% He^+ in the plasma source [11]. In the case of nitrogen admixture 20 sccm of N_2 are injected into the exposure chamber, in order to avoid ion source poisoning. Due to a lack of atomic data of nitrogen a plasma content of nitrogen ions cannot be determined.

3. Results

3.1. Plasma characterisation

The analysis of the Langmuir probe data (figure 3) is done using an automated algorithm. The algorithm connects iterations of a 50 Hz voltage sweep to their respective radial coordinate in the plasma, yielding the radial plasma profiles. Statistical errors are derived from the uncertainties of the fits and are within the thickness of the line. The plasma is seen to have the typical hollow profile of PSI-2 with maximum density and temperature about 23 mm away from the plasma centre and about 1/3 of the peak flux values in the centre. The selected plasma scenario provides a peak flux density of $9 \pm 0.5 * 10^{21}$ D m^{-2} s at an electron temperature of about 8 eV. According to these data a large span of flux densities of about a factor 9 is present on the sample during exposure. Ion impact energies are deduced from these parameters by the theory given in [13] to about $3.7 * T_e = 30$ eV in the plasma peak. To keep the ion impact energy more stable over the sample area and throughout the exposure a negative bias of 68 V is applied to the sample holder against the grounded vessel wall, resulting in ~40 eV impact energy. Besides the probe data also a biasing scan is applied to the sample holder. The floating voltage of the sample manipulator is 55 V. Above 120 V manipulator bias an ion saturation current of 1.6 A to 5.7 A = $1–3.6 * 10^{19}$ D^+ s^{-1} is measured. Via ion mass spectrometry the plasmas were characterized to consist of mainly D^+ ions.

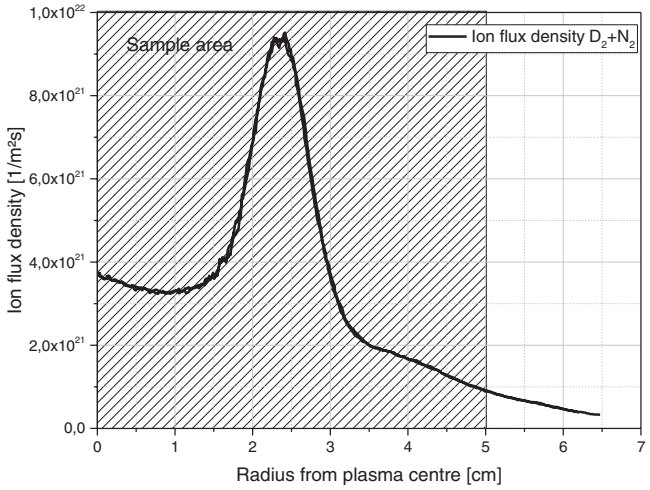

Figure 3. Representative radial plasma flux profile of the $D_2 + N_2$ exposure obtained via the Langmuir probe. A maximum flux density of about $9.3 * 10^{21}$ m^{-2} s and a mean of $4 * 10^{21}$ m^{-2} s are achieved. Over the whole sample area (shaded region) of $100 \times 80\,mm^2$ the flux density varies by a factor 9.

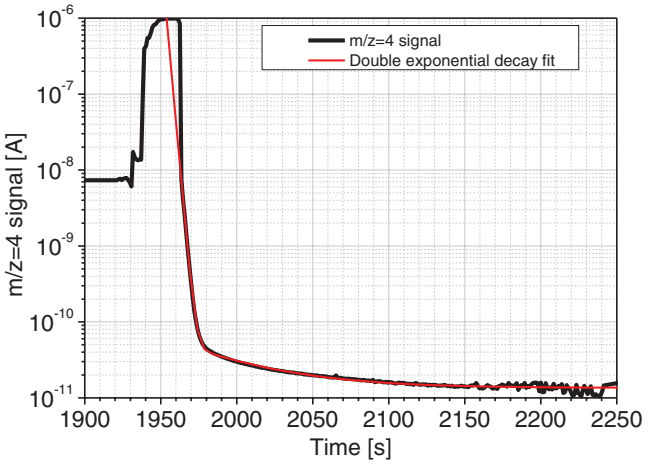

Figure 4. Plot of the pump-down of TEAC with neutral gas loaded sample and chamber. The fit indicates the presence of two decay times besides the pumping time of 58 ms. The peak at 1950s is due to the manipulator entering TEAC and thus opening the full tube diameter before the shutter is closed at 1963s. After about 10 s the signal is <10% of the typical exposed sample signal, after 200 s the background level of 10^{-11} A is reached. Instead of subtracting this curve the first 10 s of outgassing data are neglected in the outgassing experiments, due to the strong dynamics in that window.

3.2. Time-resolved QMS outgassing flux analysis

The outgassing is analysed in 10 experiments. To be able to address the effects of TEAC chamber wall outgassing and pump-out of the gas introduced into TEAC by the connection to the plasma chamber, this effect is quantified in an experiment without plasma sample loading (figure 4). The sample manipulator is moved to the usual exposure position and 150 sccm D_2 gas is introduced into the chamber to reach the same TEAC neutral pressure as under plasma conditions. These conditions are kept for 1900s, then the manipulator is moved back to TEAC and the valve between TEAC and plasma chamber is closed.

The pumping data is analysed using a double exponential function

$$y(t) = y_0 + A * e^{-t/\tau_1} + B * e^{-t/\tau_2} \quad (3)$$

Besides the pump down time constant of 58 ms mentioned earlier, time constants of $\tau_1 = 2 \pm 0.01$ s and $\tau_2 = 48.1 \pm 2$ s are found by the pump-down analysis. These additional time constants might originate from adsorption processes on the chamber walls. About 200 s after closing the shutter to the plasma chamber the background/detection limit of the QMS signal is reached. To avoid a relevant influence of the TEAC pump-down the first 10 s after closing of the TEAC valve are neglected in the data evaluation, leaving the impact of pump-down on the data <1%.

In the next step two pumping speeds are applied in TEAC in order to induce different pressures leading to different surface coverage of H and D and thus surface recombination rates during the outgassing, if the surface is not fully saturated at both pressures. The D_2 partial pressure is increased by a factor 7.4 ± 0.3 by lowering the pumping speed from 630 Hz to 210 Hz. The sample is exposed in each experiment at a peak temperature of 363 K (~373 K surface temperature) for 30 min (fluence $1.8 * 10^{22}$ D^+) and outgassed at 293 K. Unfortunately no precise calibration is available for these two experiments, as problems with the QMS required a readjustment of the device after these experiments. The same sample is exposed to these two conditions three times in a consecutive way. First the sample is pre-loaded, followed by 1 d of outgassing. After the pre-loading the first experiment using 630 Hz pumping speed is conducted, followed by the second experiment at 210 Hz on the same day. The outgassing curves are shown in figure 5. Only a minor difference is observed in the temporal decay function, probably originating from different pump-out and noise in both experiments. The integral outgassing signal (100 s–6000 s after exposure) is changed by a factor of 9 ± 0.5, which is $22 \pm 12\%$ more than the ratio of the pumping speeds. Analysis using equation (1) shows that the volume term cannot be responsible for this difference. It can be concluded that the D_2 surface recombination cannot be considered as fast compared to the diffusion. Its impact is small, but relevant for the D_2 outgassing at room temperature.

First the outgassing from a rough $100 \times 80 \times 1\,mm^3$ W plate is studied by four D_2 plasma experiments with the QMS using the SEM detector. As revealed in later experiments the SEM detector is not delivering stable signals, but variations of a factor of 2 can occur within some hours of continuous measurement. In conclusions these data have to be handled with care, but at least on the short-term valuable information is present. All exposures are run for 6 h (fluence of $7.2 * 10^{22}$ D). The data for HD ($m/z = 3$) is not shown, as the curves follow the $m/z = 4$ curves, but with a factor of 5 reduced intensity. With the applied calibration method it is not possible to get a precise calibration for HD.

All four outgassing curves are analysed using the power law function with time t

$$y(t) = y_0 + A * t^{\alpha} \quad (4)$$

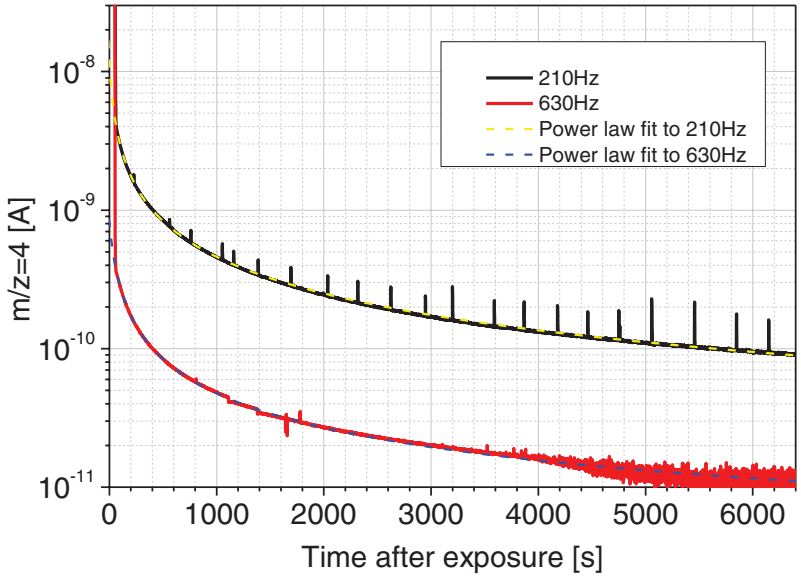

Figure 5. Time traces of the outgassing at two different pumping speeds (210 Hz and 630 Hz turbo frequency) of the W plate exposed for 30 min. The fits are in good agreement with the data ($R^2 > 0.999$). Despite the factor 9 stemming from the pressure level only a small difference in the decay behaviour ($\alpha(210\,\text{Hz}) = -0.892 \pm 0.001$ versus $\alpha(630\,\text{Hz}) = -0.915 \pm 0.001$) is observed. The differences are probably systematic errors due to the higher noise level and the different pump-out time in the 210 Hz case compared to the 630 Hz case.

Table 1. Fit values of the power law to the outgassing curves at the investigated conditions.

Conditions	Fit quality R^2	A	α	y_0	Integral D_2	D^+ fluence	Peak fluence
340 K, 7 min	0.9992	$8.8 * 10^{12}$	−1.15	$2.0 * 10^{8}$	$1.87 * 10^{13}$	$4.2 * 10^{21}$	$2.5 * 10^{24}$ D m^{-2}
360 K, 30 min	0.9901	$5.8 * 10^{11}$	−0.79	$8.9 * 10^{8}$	$7.03 * 10^{13}$	$1.8 * 10^{22}$	$1.1 * 10^{25}$ D m^{-2}
360 K, 120 min	0.9973	$2.6 * 10^{12}$	−0.79	$-3.2 * 10^{8}$	$7.63 * 10^{13}$	$7.2 * 10^{22}$	$4.3 * 10^{25}$ D m^{-2}
690 K, 30 min	0.9999	$4.7 * 10^{12}$	−0.95	$-1.6 * 10^{8}$	$3.43 * 10^{13}$	$1.8 * 10^{22}$	$1.1 * 10^{25}$ D m^{-2}

Note: the result of small, but finite y_0 is unphysical and indicates probably a long-term device drift.

Table 2. Experimental c_2 onditions and results of the outgassing fits.

Plasma composition	D_2	D_2 + 5% He ion flux	D + N_2	D_2 + 5% He + N_2
Exposure temperature	870 K	860 K	830 K	830 K
Outgassing temperature	570 K	570 K	580 K	580 K
Peak fluence density	$2.1 * 10^{26}$ D m^{-2}	$2.1 * 10^{26}$ D m^{-2}	$2.1 * 10^{26}$ D m^{-2}	$1.7 * 10^{26}$ D m^{-2}
Integral fluence	$7.2 * 10^{23}$ D	$7.2 * 10^{23}$ D	$7.2 * 10^{23}$ D	$5.8 * 10^{23}$ D
α for D_2 beginning	−0.77	Data lost	−0.25	−0.33
α for D_2 end	−2.26	−2.93	−2.35	−1.72

Note: in all cases the outgassing power law strongly varies over time with similar starting and final values. The fits can be seen in figure 7.

In the equation $t = 0$ is the time when the loading/plasma is stopped. The first usable data point is at $t = 60$ s after the exposure. All fits yield a very good agreement to the data ($R^2 > 0.99$), especially when comparing with exponential decay fits. The results of fitting and integration are presented in figure 6 and table 1 for the data points from 60 s to 55 000 s.

The next set of four exposures is conducted with constant temperature and fluence, but varying plasma composition in order to check whether the power law (equation (4)) is still applicable under different surface conditions and chemistry at elevated temperature. In these experiments both QMS are operated with Faraday detector. A rough $100 \times 80 \times 5\,\text{mm}^3$ W mask is used in all exposures equipped with seven $10 \times 10 \times 5\,\text{mm}^3$ rough dummy samples and 1 polished sample for post-analysis. The samples are exposed for 6 h, except for the $D_2 + He + N_2$ sample which is aborted after 5.2 h due to a technical failure. Details of the exposure conditions and outgassing results can be found in table 2.

The D_2 outgassing does not behave according to equation (4), but shows a constant change of the α parameter (figure 7). The outgassing of $m/z = 20$ and 28 shows in all cases a similar behaviour, as visible in figure 8. These masses are dominant in the base pressure and do not show as strong dynamics as D_2. Also, $m/z = 3$ typically shows the same behaviour as $m/z = 4$, but with about 30 times lower signal intensity. In the $D_2 + N_2$ and $D_2 + He + N_2$ cases $m/z = 20$ is observed, reaching the detection limit after 100 000 s in the first and after 10 000 s in the latter case. The outgassing of

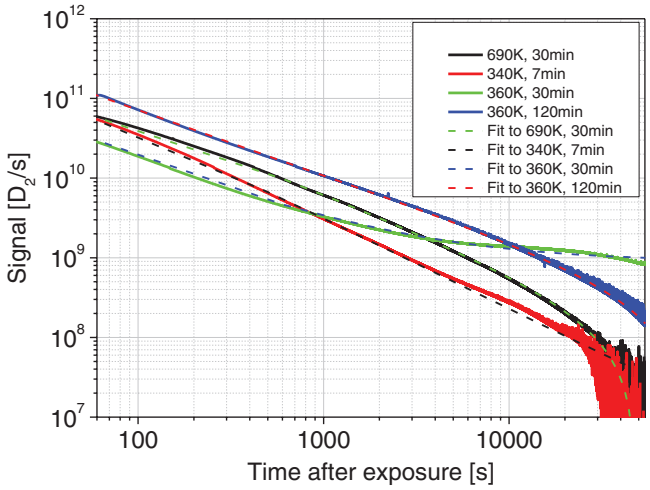

Figure 6. The calibrated outgassing after three different fluences/exposure times and two different temperatures. All curves are fitted by t^{α} power laws (dotted lines). For all conditions deviations from the straight line predicted by t^{α} occur in the end of the outgassing measurement. This behaviour can only be reproduced by using unphysical values of y_0 and is probably an artifact of the SEM detector drift.

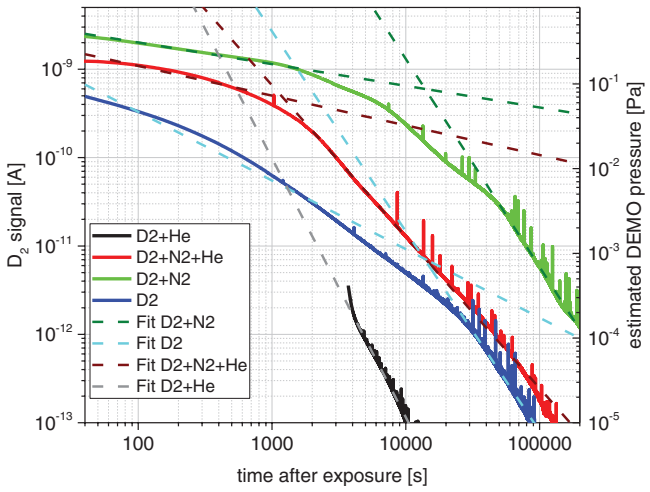

Figure 7. D_2 outgassing rate evolution after four different plasma exposures at ~900 K acquired with the Prismaplus QMS. Outgassing is done at ~580 K. Fits indicate the decrease of α over time. The contribution of He to the cases where He is present is in the percent range. The DEMO pressures are estimated with 2000 m^2 and 100 $m^3\ s^{-1}$ (section 4).

helium is only observed in the $D_2 + He$ and $D_2 + N_2 + He$ cases, where the amount is about 1% of the D_2 value.

3.3. Post analysis

Post-analysis is performed using thermal desorption spectrometry (TDS), nuclear reaction analysis (NRA) and electron microscopy using SEM + EDX + FIB on the single polished sample of each high temperature exposure. For the low temperature exposures no post-analysis is performed, as no surface analysis samples are available (full plates are exposed). Besides that no changes in surface morphology are visible and also no differences are expected as the conditions are rather similar.

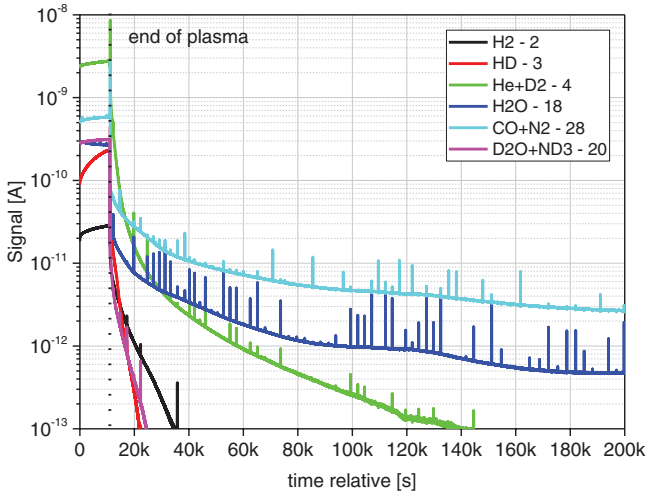

Figure 8. Example plot of the signal intensities of the Prismaplus of different masses during and after $D_2 + N_2 + He$ experiment. The plasma stops at 11 160 s. Typical molecules are associated to the integer m/z values in the legend. In contrast to figure 7 the red D_2 line gives a different impression, because of different zero time and x-scaling selection.

The FIB + SEM analysis shows a 205 ± 5 nm thick fuzz layer on the $D_2 + He$ exposed samples, which is not formed in the $D_2 + He + N_2$ case, see figure 9. Despite the ion energy being below the sputtering threshold for W a grain orientation dependent surface modification and erosion is observed on the samples without fuzz. The modification seems to follow crystal planes and may be induced by ad-atom formation and diffusion rather than sputtering. In all except the $D_2 + He$ case open blisters can be found. While in the D_2 case only tiny nm size holes are found in the ripples of the surface modification, some hundred nm large holes are found on the $D_2 + N_2$ sample which are even larger and more frequent in the $D_2 + He + N_2$ case. The energy dispersive x-ray (EDX) spectroscopy with 3 keV electrons reveals peaks for W, O and N in the range of 0–3 keV. In pure and dense W a probing depth of 20 nm [14] is obtained in these measurements. In the case of pure D_2 plasma no N is observed above the background. In all other cases 6% N are found within the probing depth, but a partial overlap with the larger O peak complicates the error estimation. For the fuzz sample $37 \pm 0.4\%$ of O are found, while the other samples are similar at $9.2 \pm 0.2\%$.

The NRA analysis using 2.94 MeV ^{3}He ions with a two detector setup at 165° scattering angle and SimNRA6.06 [15] for data evaluation reveals the implantation of C [16], O, N and D [17] in the samples (table 3). The N content cannot be quantified due to the lack of cross-section data in the literature, but relative factors given by reaction rates are still valid, for thin surface layers. For the O content a rough number with a systematic error of a factor 2 is given by the comparison to TiO_2 oxygen signal levels. The measurement is done about 1 month after exposure. The depth profiling shows clear surface contaminations of C, O, N typical for PSI-2 D_2-plasma exposures. Only in the case of the fuzz layer on the $D_2 + He$ sample $a \sim 10$ times higher impurity content is observed, probably due to absorption from the air after exposure. The NRA impurity analysis thus leads to similar results as the EDX

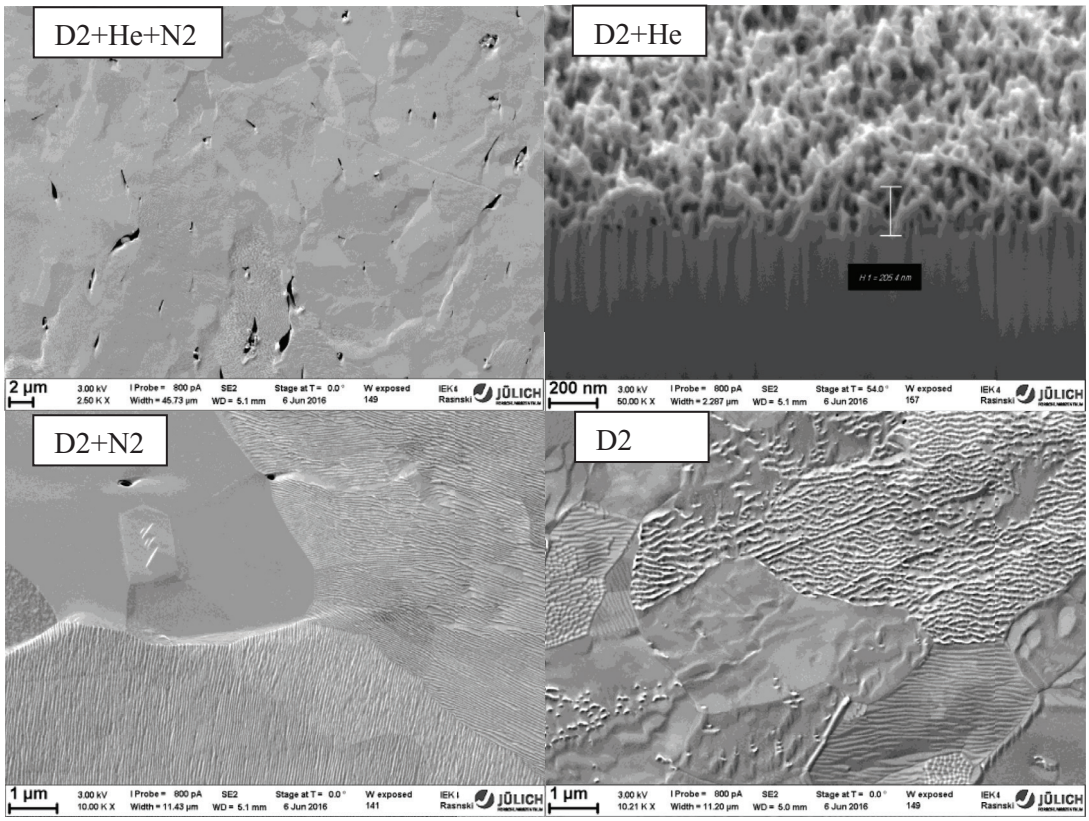

Figure 9. FIB cross-section of the fuzz produced on the $D_2 + He$ exposed sample with a thickness of 205 nm (top-right). The pictures of $D_2 + N_2$ and $D_2 + He + N_2$ have a rather similar impression with open blisters and some crystal plane erosion in certain grain orientations. In the pure D_2 exposure the crystal plane erosion is also visible, but holes cannot be found.

Table 3. NRA (first 4.2 μm) and TDS (full sample) results for the retention of D_2, He and surface impurities (C, N, O within first 0.8 μm).

	NRA (10^{19} atoms m^{-2})								TDS (10^{19} atoms m^{-2})	
Experiment	C	O	N (a.u.)	D (<0.8 μm)	D (0.8–4.2 μm)		Sum D (0–4.2 μm)		D	He
D_2	10.4	7.9	27	0.024	0.035	±0.025	0.059	±0.024	2.4	0
$D_2 + N_2$	14.9	7.8	160	0.122	0.108	±0.041	0.23	±0.058	9.36	0
$D_2 + N_2 + He$	13.1	6.3	137	0.297	0.106	±0.025	0.403	±0.101	5.9	17
$D_2 + He$	75.9	101.8	167	0.313	0.263	±0.062	0.576	±0.078	0.77	25.4

Note: in NRA a detection limit of $1.5 * 10^{17}$ D m^{-2} is realized with uncertainties of typically 15%. The addition of N_2 strongly increases the D retention up to a factor of 4 (8 in first 4.2 μm). In the $D_2 + He$ case the total retention is reduced by a factor 3 and nearly completely located in the first 4.2 μm, indicating a strong diffusion barrier effect induced by the retained He. The same effect is observed when comparing $D_2 + N_2$ and $D_2 + N_2 + He$ where the He is strongly retained, slightly reducing the total retention while concentrating it at the surface. The retention of N is not quantified due to the lack of NRA cross-sections. He fuzz strongly accumulated surface impurities, most probably during transfer through air after the experiment.

analysis. The long-term retention of D in the first 4.2 μm is clearly increased by up to a factor 10 by adding the impurities to the D_2-plasma. Due to the low D content not enough counts could be acquired for a detailed depth profile, but only 2-point profiles (0–0.8 μm and 0.8–4.2 μm) can be obtained. Except for the $D_2 + N_2 + He$ case no significant variation with depth is present. The addition of N to the plasma clearly increases the near-surface N concentration in the samples, indicating a nitride formation as also supported by the EDX analysis. A deep diffusion of N (below the first resolution point) is not observed within the NRA detection limit.

One month after NRA analysis the samples are outgassed in a TDS device and the outgassing is monitored by QMS for D_2 ($m/z = 4.03$), He ($m/z = 4$) and N_2 ($m/z = 28$) rates up to 1200 K with 0.2 K s^{-1} using the same QMS types as in TEAC. The results are summarised in figure 10 and table 3. All outgassing <900 K can hardly be exposure related (~900 K exposure temperature), which mainly affects the N_2 and H_2 interpretation.

A $m/z = 28$ peak at about 1100 K is seen on all samples, but with about 3 × higher magnitude in the N_2 exposed samples, compared to the D_2 and $D_2 + He$ cases. The $m/z = 28$ signal of N_2 can be influenced primarily by CO, while the $m/z = 14$ signal is also affected by NH_3, CH_4 and their deuterated compounds. The signals thus have to be considered with care, but as 28 and 14 are evolving in parallel, with 28

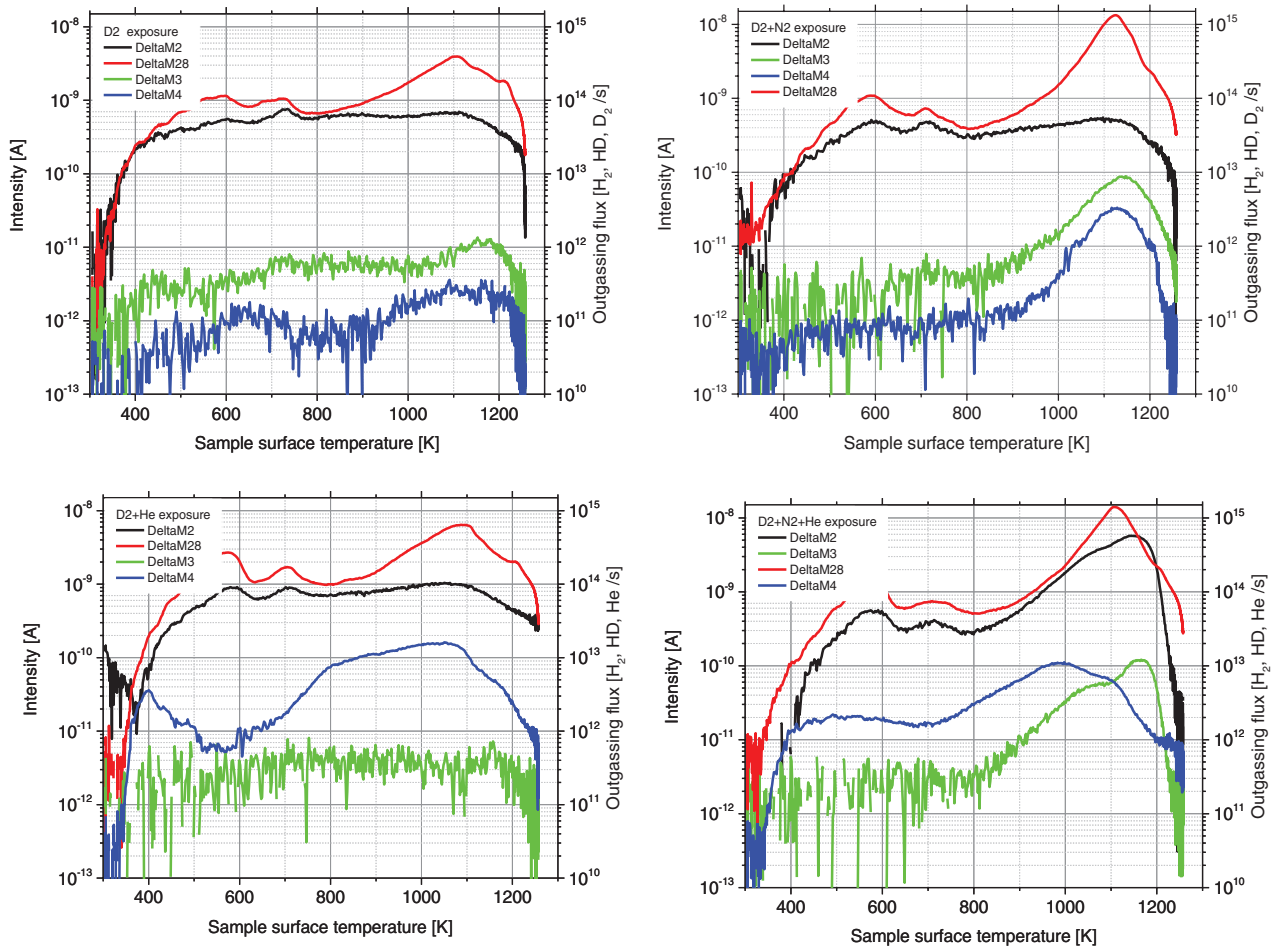

Figure 10. TDS spectra of the samples exposed to mixed PSI-2 plasmas acquired at 0.2 K s^{-1}. In all cases only H_2, HD, D_2 and He outgassing are quantified, N_2 remains in arbitrary units. Significant D_2 outgassing is found only in the D_2 and $D_2 + N_2$ cases, where no He outgassing is found. In both He admixed cases only He, but no D_2 outgassing is found. Outgassing peaks below about 900 K can hardly be related to the experiment, as this is the exposure temperature. While for deuterated molecules and He basically no outgassing is observed in that region, H_2 and N_2 are showing desorption peaks. From this data it could be recommended to operate W based materials >1100 K in order to further reduce N, He and D retention.

being about 10 × higher at the peaks at 1100 K, this part is considered to be N_2 dominated. In conclusion also nitrogen is desorbing from the materials even if an intense background is present in the W samples, maybe due to manufacturing. In the $D_2 + N_2 + He$ and $D_2 + He$ cases He is observed in $m/z = 4.0$ while deuterium is not outgassed as D_2 in $m/z = 4.03$, but only as HD in $m/z = 3$. For He outgassing from the $D_2 + He$ sample a strong flux is observed already slightly below the exposure temperature, similar to [18]. In all cases strong H_2 signals are found roughly in parallel to the HD outgassing with levels 1–2 orders of magnitude above the deuterium related signals. Only about 20% of this H_2 outgassing is related to the TDS background (figure 11). In conclusion a relevant isotope exchange of H and D can be assumed in the 2 month after exposure, as the H_2 outgassing directly after exposure is about 10 times smaller compared to the D_2 outgassing (figure 8). Generally the results show that most of the D_2 is outgassed during the in-vacuo outgassing (high dynamic inventory) and most of He and N are retained long-term (small dynamic inventory at 580 K).

4. Discussion in DEMO context

For a future fusion reactor DEMO one of the main questions to be addressed here is how long it takes in between two discharges to pump-down the vacuum vessel for a new plasma breakdown to be possible. As DEMO could be made with full tungsten plasma-facing components operating at about 1000 K surface and 550 K coolant temperature no current tokamak can provide a reasonable estimate of the outgassing fluxes and corresponding pressures. Modelling tries to fill this gap. The data presented here are intended for a model validation as the experimental conditions are well-defined and new data close to the planned DEMO conditions were presented in the last sections. The impact of radiation damage on the outgassing cannot be addressed here, though.

It was attempted to explain the tokamak observations of $\alpha \approx -0.7$ [6, 7] by the complex conditions of a tokamak, folding several materials and loading conditions into one parameter (the D_2 partial pressure evolution). In the data presented here this complexity is now substantially reduced with just one material and temperature and reduced flux density

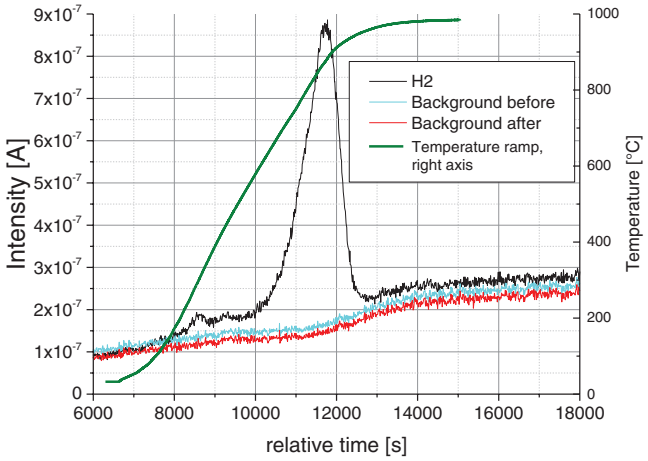

Figure 11. Signal to background comparison of the H_2 outgassing of the $D_2 + N_2 + He$ sample during temperature ramping. The H_2 flux is about 100 times higher than the HD flux (figure 10) and is clearly above the device background, thus related to the outgassing from the sample.

variations (factor 9) over the sample area. The model in [6] predicts for such a clean situation $\alpha = -0.5$ for the initial outgassing which gradually transforms to $\alpha = -1.5$ (diffusion limitation) in the final outgassing stage. The room temperature data are perfectly fitted with a single $\alpha \approx -1$ for 3 orders of magnitude in outgassing time, not in agreement with this model. In contrast to that, the second experimental set with high temperature outgassing shows behaviour partially in line with this model. In the beginning α is -0.25 to -0.35, but after some 1000 s after exposure the value strongly decreases to -1.72 to -2.35. The simple power-law fit is not describing the data correctly, but instead a transition from a probably diffusion limited ($\alpha = -0.5$) to a recombination limited ($\alpha = -2$) outgassing takes place within the observation time. Modifications to the strict values could be induced by the initial D filling depth profile as proposed in [10]. In the case of elevated temperatures the shift from diffusion to recombination limitation is accelerated and becomes observable, while for outgassing at room temperature a certain ratio between the processes seems to be stable in the dynamic range (intensity and time) of the measurement technique, keeping the process in an intermediate state. This is supported by the observation of a slight impact of surface coverage on the outgassing rate at room temperature, suggesting a nearly complete coverage of the surface with D (figure 5).

Using the new data and the technical parameters foreseen for DEMO [19] an estimate of the pump-down time after a plasma discharge can be given for the different impurity scenarios. As QMS calibrations for ammonia and water are not available and helium outgassing is fast, the calculations are based only on the D_2 outgassing, thus giving a lower limit for the pump-down time. From the other masses observed during outgassing and the surface analysis results it can be estimated that D_2 contributes >90% to the partial pressure, especially in the first 10 000 s. The systematic error of this approximation is thus believed to be small. In a DEMO with a plasma loaded surface of 2000 m^2 and a pumping speed of 100 $m^3\ s^{-1}$ a pump-down to $5 * 10^{-4}$ Pa is possible within 1 h ($D_2 + He$), 3 h (D_2), 5 h ($D_2 + N_2 + He$) and 33 h ($D_2 + N_2$), respectively. These numbers are extrapolated from the high temperature PSI-2 experiments, as demonstrated on the right *Y*-axis of figure 7. With the outgassing being D_2 (+T) dominated, a plasma restart in DEMO could be possible without any extra gas injection for purification.

The new data are not supportive for the model presented in [8]. According to that model α depends on the reaction order (2 for molecular desorption) and the density of possible states for the hydrogen in the material. As the reaction order is fixed and the material used here is always the same, this density of states must, according to the experimental results, depend on the exposure time and temperature and also vary with outgassing time in a complex function, which seems unlikely. As an extension of the model presented in [6] also anomalous diffusion might be considered. Anomalous diffusion can occur if the transport of the retained deuterium to the surface is hindered by spatially fixed obstacles [20]. This description is implicitly included in reaction-diffusion models including trapping, as e.g. the CRDS model [10]. In the case of tungsten, bubbles, surface layers and helium retention indicate strong trapping sites which are also found in surface analysis. The CRDS model can explain the observations of α varying between -0.25 and -2.35 by the change of the deuterium loading profile during the outgassing and the transition between diffusion and recombination limitation [10]. A theoretical assessment of outgassing fluxes and pump-down times for DEMO will thus strongly depend on the in vessel location and plasma and material conditions.

5. Conclusions

The outgassing of 99.96% pure tungsten is analysed via in-vacuo quadrupole mass spectrometry in the time frame of 40 s to about 170 000 s after deuterium and mixed plasma loading for up to 6 h in PSI-2. Temperatures, fluxes and fluences are chosen to cover ranges of current tokamak and future DEMO conditions. Surface and retention analysis is performed on selected samples to connect the observations of outgassing with actual modifications of the materials.

The new results presented here break down the complex outgassing situations in tokamaks to a single material and single temperature system with virtually infinite pumping speed (58 ms pumping time constant). Nonetheless the results show basically the same temporal behaviour, a t^{α} power-law, as the tokamak results, if outgassing happens at room temperature. With loading at ~900 K and outgassing at 570 K sudden breaks in the exponents appear during outgassing, the power-law is not a valid description anymore. Values for the exponent α of -0.25 (directly after exposure) to -2.35 (end of outgassing) are observed. This change in behaviour could be attributed to the deuterium depth profile and the interplay of the temperature dependent reaction-diffusion processes, leading only in special situations (e.g. room temperature) to an effective power-law.

The outgassing rate and sum are higher for both N_2 admixed cases which also show increased long-term retention compared to the D_2 and $D_2 + He$ cases. In contrast, He admixture

reduces the long-term retention and outgassing flux in both cases. Probably the fuzz and nitride surface layers act as a diffusion barrier leading to a higher dynamic inventory during the long exposures at ~900 K (full sample loading). The fuzz and/or the retained He more effectively prevents deep D diffusion compared to N, as indicated by NRA. The mobile part of the deuterium inventory is smaller in the case of fuzz and $D_2 + N_2 +$ He (high surface defect/blister density) leading to a relative decrease in the release rates and an increase in the surface near D-retention.

After exposure to D_2 plasmas admixed with N_2 and/or He the general time evolutions are similar to the pure D_2 plasma exposure, but with different coefficients. The application of the present deuterium outgassing models for more complex plasma composition scenarios thus seems possible only qualitatively. A pathway for quantitative improvement could be the inclusion of modified surface layers (e.g. nitrides, fuzz) and the interaction of the different implanted species as indicated by post-analysis, where significant He and N retention is found. The outgassing fluxes of other species (He, ND_3…) are most probably $<10\%$ of the total flux.

The observations suggest that for a DEMO reactor the pump-down time in between two pulses strongly depends on the composition of the plasma. In the case of fuzz growth with $D_2 +$ He plasmas 1 h can be sufficient to reach 5 mPa, while for N_2 admixture this time could increase to 5 h for a DEMO design with 2000 m^2 plasma-facing surface area and 100 $m^3\ s^{-1}$ pumping speed. Possible solutions are lower impurity content and higher pumping speed, the use of other, non-tungsten materials (e.g. RAFM steels) for plasma-facing surfaces, higher allowed plasma start-up pressures or significantly longer pulses (Stellarator DEMO).

The perspective of this kind of measurements offers possibilities with more systematic temperature, ion flux and sample material variations as well as the important combination with modelling to gain further insight into the physics of gas retention and release in plasma-facing materials.

Acknowledgments

The authors thank the PSI-2 Team, especially Michael Vogel, Sebastian Kraus and Thorsten Tietz for the reliable device operation and preparatory works for the LID facility. The authors thank Michaele Freisinger for supporting the mass spectrometer measurements.

This project has received funding from the European Union's Horizon 2020 research and innovation programme under grant agreement number 633053. The views and opinions expressed herein do not necessarily reflect those of the European Commission.

References

[1] Rieth M. *et al* 2013 Recent progress in research on tungsten materials for nuclear fusion applications in europe *J. Nucl. Mater.* **432** 482–500
[2] Anderl R.A., Holland D.F., Longhurst G.R., Pawelko R.J., Trybus C.L. and Sellers C.H. 1992 Deuterium transport and trapping in poly-crystalline tungsten *Fusion Technol.* **21** 745–52
[3] Frauenfelder R. 1969 Solution and diffusion of hydrogen in tungsten *J. Vac. Sci. Technol.* **6** 388
[4] Poon M., Haasz A. and Davis J. 2008 Modelling deuterium release during thermal desorption of D^+ irradiated tungsten *J. Nucl. Mater.* **374** 390–402
[5] Causey R., Wilson K., Venhaus T. and Wampler W.R. 1999 Tritium retention in tungsten exposed to intense fluxes of 100 eV tritons *J. Nucl. Mater.* **266–269** 467–71
[6] Philipps V. and Ehrenberg J. 1993 Analysis of outgassing after Joint European Torus discharges under beryllium first wall conditions *J. Vac. Sci. Technol.* A **11** 437–45
[7] Brezinsek S. *et al* 2013 Fuel retention studies with the ITER-like wall in JET *Nucl. Fusion* **53** 083023
[8] Smirnov R., Krasheninnikov S.I., Guterl J., Baldwin M.J. and Doerner R.P. 2014 Modeling of hydrogen retention and outgassing from co-deposits with distributed energy states *Contrib. Plasma Phys.* **54** 610–4
[9] Andrew P. and Pick M. 1995 Hydrogen retention in the first wall *J. Nucl. Mater.* **220–2** 601–5
[10] Matveev D., Wensing M., Möller S., Kreter A., Brezinsek S. and Linsmeier C. 2016 Hydrogen outgassing following plasma exposure *Nucl. Mater. Energy* submitted
[11] Reinhart M. 2015 *Influence of Impurities on the Fuel Retention in Fusion Reactors* (Germany: Forschungszentrum Jülich GmbH) (http://juser.fz-juelich.de/record/281952/files/Energie_Umwelt_296.pdf) ISBN 978-3-95806-105-7
[12] Kreter A., Brandt C., Huber A., Kraus S., Möller S., Reinhart M., Schweer B., Sergienko G. and Unterberg B. 2015 Linear plasma device PSI-2 for plasma-material interaction studies *Fusion Sci. Technol.* **68** 8–14
[13] Emmert G., Wieland R., Mense T. and Davidson J. 1980 Electric sheath and presheath in a collisionless, finite ion temperature plasma *Phys. Fluids* **23** 803
[14] Drouin D. www.gel.usherbrooke.ca/casino/ Sherbrooke University (Online)
[15] Mayer M. 1997 *SimNRA User's Guide IPP Report Number*: IPP 9/113 Garching, Max-Planck-Institut für Plasmaphysik (www.simnra.com)
[16] Kuan H.M. and Bonner T.W. 1964 An investigation of the $C_{12} + He_3$ reactions at bombarding energies between 1.8 and 5.4 MeV *Nucl. Phys.* **51** 481
[17] Alimov V.K., Mayer M. and Roth J. 2005 *Nucl. Instrum. Methods* **B234** 169
[18] Lee H., Haasz A., Davis J. and Macaulay-Newcombe R. 2007 Hydrogen and helium trapping in tungsten under single and sequential irradiations *J. Nucl. Mater.* **360** 196–207
[19] Battes K., Day C. and Rohde V. 2015 Basic considerations on the pump-down time in the dwell phaseof a pulsed fusion DEMO *Fusion Eng. Des.* **100** 431–5
[20] Berry H. and Chaté H. 2014 Anomalous diffusion due to hindering by mobile obstacles undergoing Brownian motion or Orstein–Ulhenbeck processes *Phys. Rev.* E **89** 022708